



OPEN ACCESS

EDITED BY
Yefei Ren,
Institute of Engineering Mechanics, China
Earthquake Administration, China

REVIEWED BY
Haiping Ding,
Suzhou University of Science and
Technology, China
Zhinan Xie,
Institute of Engineering Mechanics, China
Earthquake Administration, China

*CORRESPONDENCE
Yushi Wang,
✉ wangyushi@bjut.edu.cn

SPECIALTY SECTION
This article was submitted to
Structural Geology and Tectonics,
a section of the journal
Frontiers in Earth Science

RECEIVED 30 November 2022
ACCEPTED 20 December 2022
PUBLISHED 10 January 2023

CITATION
Wang Y, Ding Y and Li X (2023), Scaling
ratios for spectral accelerations caused by
seismic site effect under site condition
classifications in China.
Front. Earth Sci. 10:1112202.
doi: 10.3389/feart.2022.1112202

COPYRIGHT
© 2023 Wang, Ding and Li. This is an open-
access article distributed under the terms
of the [Creative Commons Attribution
License \(CC BY\)](https://creativecommons.org/licenses/by/4.0/). The use, distribution or
reproduction in other forums is permitted,
provided the original author(s) and the
copyright owner(s) are credited and that
the original publication in this journal is
cited, in accordance with accepted
academic practice. No use, distribution or
reproduction is permitted which does not
comply with these terms.

Scaling ratios for spectral accelerations caused by seismic site effect under site condition classifications in China

Yushi Wang*, Yi Ding and Xiaojun Li

Key Laboratory of Urban Security and Disaster Engineering of China Ministry of Education, Beijing University of Technology, Beijing, China

The spectral accelerations (S_a), which are widely used as ground motion inputs in structural seismic designing, are significantly affected by local site conditions classified by near-surface geology. A novel approach of quantifying the scaling ratios for S_a on site class I, II, III, and IV under the site condition classifications in Chinese seismic codes, was proposed. In this integrated approach, the scaling ratios for S_a on each site class were subordinated to three constituents, i.e., scaling ratios for peak ground acceleration (PGA), scaling ratios for PGA-normalized S_a , and non-linear decay exponents. The scaling ratios for peak ground acceleration were derived from recent studies and numerical simulations of 1,138 borehole models in China, the scaling ratios for PGA-normalized S_a were derived from 3,584 strong motion records in NGA West two database, and the non-linear decay exponents were derived from about 140 thousand borehole observation data recorded by KiK-net. Consequently, this approach was solidly based on statistics of observation data in company with numerical simulations, which resulted in more reasonable and more reliable scaling ratios for S_a caused by the seismic site effect under site condition classifications in China.

KEYWORDS

seismic site effect, local site condition, site scaling ratio, near-surface geology, spectral acceleration, strong motion record, NGA West 2 database, KiK-net

1 Introduction

Seismic damage data and strong motion records showed that local site conditions have a significant impact on the characteristics of ground motions, especially the medium-to-long period components are significantly amplified by soft overburdens, which should be sufficiently considered during the determination of ground motion inputs for structural seismic designing (Seed et al., 1969; Hu et al., 1980; Aki, 1993; Hu, 2006). For an important engineering structure, it is generally necessary to carry out engineering geological survey, establish a local site model, and conduct numerical simulation of site seismic response considering the influence of seismic environment, strong motion attenuation, and other factors to determine the ground motion inputs related to the local site condition. Meanwhile, for general projects with large quantities and a wide range of areas, it is necessary to establish the scaling ratios for ground motion induced by the seismic site effect on homologous site conditions for the convenience of engineering applications (Li et al., 2001a; Stewart and Seyhan, 2013; Bo et al., 2021).

Based on the site condition classifications in China, different scaling ratios for ground motion parameters caused by the seismic site effect were given (Lu et al., 2008; Li, 2013), in which the ground motion parameter most commonly concerned was peak ground acceleration (PGA), while effective peak acceleration (EPA) and spectral acceleration (S_a) were also frequently used. The research methods included the conversion of foreign achievements (Lü et al., 2007), the numerical simulation of borehole models (Li et al., 2001b; Lan et al.,

TABLE 1 Site condition classification criteria in China.

V_S or V_{SE} ($m \cdot s^{-1}$)	I_0	I_1	II	III	IV
	Overburden thickness (m)				
$V_S > 800$	0	—	—	—	—
$800 \geq V_S > 500$	—	0	—	—	—
$500 \geq V_{SE} > 250$	—	<5	≥ 5	—	—
$250 \geq V_{SE} > 150$	—	<3	3–50	>50	—
$V_{SE} \leq 150$	—	<3	3–15	15–80	>80

2012), and statistics based on strong motion records in western United States (Bo, 1998; Geng, 2005; Liu et al., 2009; Zhao et al., 2009) or Japan (Guo et al., 2011; Cui et al., 2016; Bian et al., 2017), but there were obvious inconsistencies among these results.

Based on the strong motion records now available, a novel approach of quantifying the scaling ratios for S_a under the site condition classifications in China were proposed in this study.

2 Site condition classifications

2.1 Site condition classifications in China

According to “GB 50011: Code for Seismic Design of Buildings” in China (General Administration of Quality Supervision, Inspection and Quarantine of the People's Republic of China, 2016), site conditions were classified into I_0 , I_1 , II, III, and IV in accordance with shear-wave velocity and overburden thickness, as shown in Table 1, where V_S was the shear-wave velocity of the surface rock on the rock site, V_{SE} was the equivalent shear-wave velocity on the soil site. V_{SE} was defined as following:

$$V_{SE} = \sum_{i=1}^n (d_i) / \sum_{i=1}^n (d_i / V_{Si}) \quad (1)$$

where d_i was the thickness of the i^{th} layer of soil within the shallower of overburden thickness and 20 m, and V_{Si} was shear-wave velocity of the i^{th} layer of soil.

2.2 Site condition classifications in this study

The shear-wave velocity structures of the 1,138 borehole models and 140 thousand KiK-net observation data were available, and therefore the corresponding site class could be determined according to Table 1. But in the NGA West two database, the shear-wave velocity structures were not listed, hence the empirical relationship between V_{S30} (the time-averaged shear-wave velocity to 30 m depth in $m \cdot s^{-1}$) and V_{S20} (the time-averaged shear-wave velocity to 20 m depth in $m \cdot s^{-1}$) (Boore, 2004)

$$\log_{10}(V_{S30}) = 0.025439 + 1.0095 \log_{10}(V_{S20}) \pm 0.03018 \quad (2)$$

was used to classify the site conditions. If V_{S20} was treated to be identical to V_{SE} , it could be calculated that $V_{S30} > 562 m \cdot s^{-1}$ on site

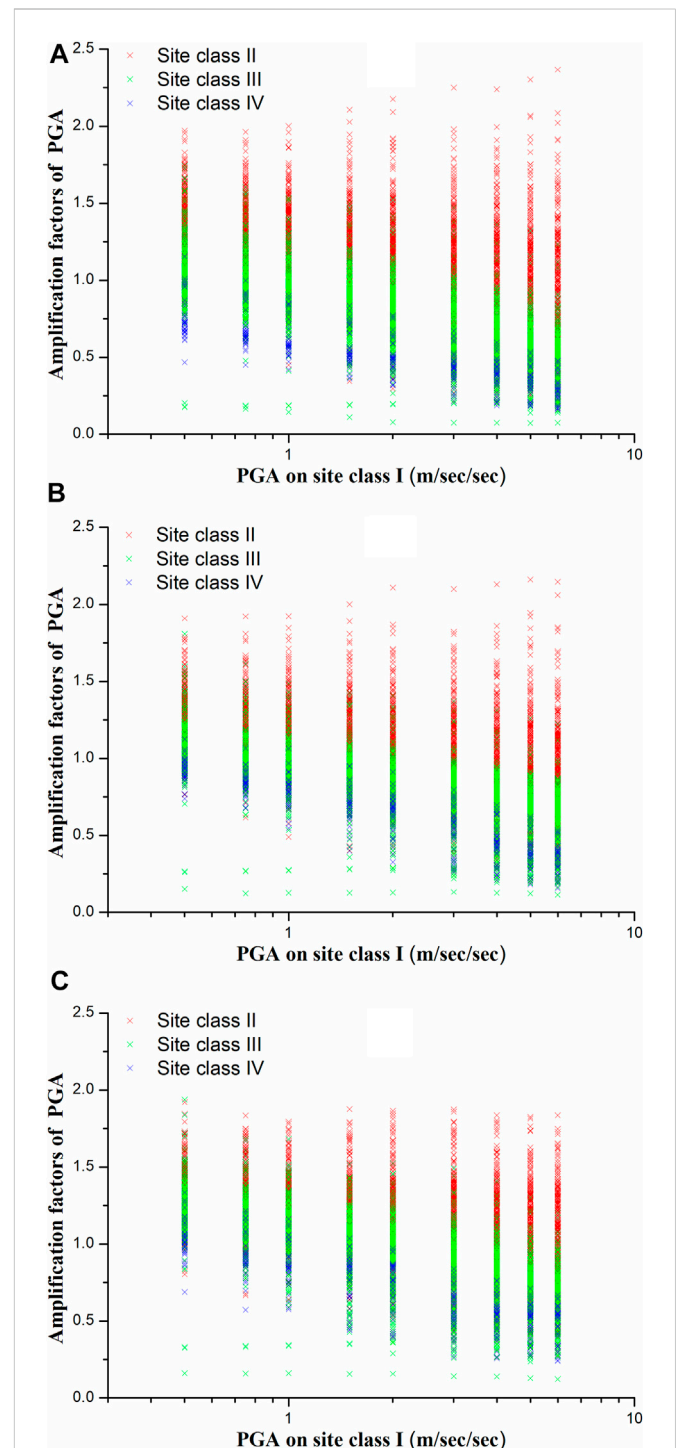


FIGURE 1
PGA amplification factors on site class II, III, and IV versus on site class I_0 given by borehole numerical simulations when the motion inputs of subterranean bottom interface were artificial acceleration time series synthesized according to the average PGA-normalized S_a for (A) $M_W = 5.0-6.0$, (B) $M_W = 6.0-7.0$, and (C) $M_W = 7.0-8.0$.

class I, $562 m \cdot s^{-1} \geq V_{S30} > 280 m \cdot s^{-1}$ on site class II, $279 m \cdot s^{-1} \geq V_{S30} > 167 m \cdot s^{-1}$ on site class III, and $V_{S30} < 167 m \cdot s^{-1}$ on site class IV under the site condition classification criteria in China. As a result of data insufficiency, the site class I_0 was not subdivided from site class I in the following statistics.

TABLE 2 Fitting coefficients for PGA amplification factors given by numerical simulations.

Sit class	PGA-normalized Sa input	<i>a</i>	<i>b</i>	σ
Sit class II	$M_W = 5.0-6.0$	1.3648	-.4086	.2869
	$M_W = 6.0-7.0$	1.2523	-.3029	.2269
	$M_W = 7.0-8.0$	1.3757	-.3275	.2284
	Total	1.3322	-.3464	.2534
Sit class III	$M_W = 5.0-6.0$	1.0821	-.5388	.1721
	$M_W = 6.0-7.0$	1.0578	-.4141	.1536
	$M_W = 7.0-8.0$	1.2292	-.5202	.1704
	Total	1.1231	-.4911	.1793
Sit class IV	$M_W = 5.0-6.0$.7474	-.4130	.1040
	$M_W = 6.0-7.0$.9412	-.5388	.1043
	$M_W = 7.0-8.0$	1.0301	-.5312	.1291
	Total	.9062	-.4946	.1443

3 Scaling ratios for PGA

3.1 Numerical simulations of borehole models

One-dimensional equivalent linearization models for 492 boreholes on site class II, 596 boreholes on site class III, and 50 boreholes on site class IV drilled in Sichuan, Yunnan, Xinjiang and Eastern China, were established. The strong motion inputs of subterranean bottom interface were artificial acceleration time series synthesized according to the average PGA-normalized Sa on site class I for moment magnitude 5.0–6.0, 6.0–7.0, and 7.0–8.0 as shown in Figure 3 scaled by $PGA = .5, .75, 1.0, 1.5, 2.0, 3.0, 4.0, 5.0, \text{ and } 6.0 \text{ m/s}^2$. The amplification factors of PGA induced from the numerical

simulation results were shown in Figure 1. The linear fittings for amplification factors of PGA under semi-logarithmic coordinates were calculated. The linear fittings formula was

$$A_i = a + b \log_{10} \frac{PGA_i}{0.5} \pm \sigma \quad (3)$$

where the site class $i = \text{II, III, or IV}$, A_i was the amplification factor on site class i versus on site class I_0 , PGA_i was the peak ground acceleration on site class I_0 in meter/s/second (m s^{-2}), and the coefficients a , b and standard deviation σ were listed in Table 2.

3.2 Statistical results in recent studies

PGA amplification factors proposed in recent studies when $PGA \leq .5 \text{ m s}^{-2}$ on site class I_1 were listed in Table 3, and the PGA amplification factors on site class II, III, and IV versus site class I_1 were shown in Figure 2. Considering the differences between the site class I_0 and the site class I_1 , the PGA amplification factors given by numerical simulations in Table 2 were divided by 0.80 according to Table 5. It could be concluded that PGA amplification of soft overburden layers had reached consensus, but the specific values of amplification factors were not identical in different studies, even when the ground motion strength was weak enough to ignore the soil non-linearity (Wang et al., 2022).

3.3 Proposed scaling ratios for PGA

The median values of PGA amplification factors when $PGA \leq .5 \text{ m s}^{-2}$ on site class I_1 in recent studies shown in Table 3, i.e., 1.00 on site class I_1 , 1.39 on site class II, 1.30 on site class III, and 1.16 on site class IV, were proposed to be the PGA scaling ratios as a temporary compromise. The PGA scaling ratio on site class I_0 was proposed to be .80 according to the practices of NEHRP (Stewart and Seyhan, 2013).

TABLE 3 PGA amplification factors when $PGA \leq .5 \text{ m s}^{-2}$ on site class I_1 in recent studies.

Recent study	Site class I_1	Site class II	Site class III	Site class IV	Statistical data
Bo (1998)	.98	1.00	.99	—	235 strong motion records in Western United States
Li et al. (2001b)	1.00	1.50	1.10	.80	188 borehole models in China
Geng, (2005)	.53	1.00	2.00 [#]	.74	470 strong motion records in Western United States
Lü et al. (2007)	.80	1.00	1.20	1.60 [#]	Dozens of borehole models in United States
Zhao et al. (2009)	1.00	1.00	3.00 [#]	—	812 strong motion records in United States
Liu et al. (2009)	1.00	—	—	1.16	728 strong motion records in Western United States
Guo et al. (2011)	1.00	1.80	1.29	1.10	484 strong motion records in Japan
Lan et al. (2012)	.96	1.30	1.25	1.29	235 borehole models in China
Cui et al. (2016)	.70	1.00	.90	—	1,609 strong motion records in Japan
Bian et al. (2017)	.80	1.00	1.20	1.15	1,233 strong motion records in Japan
This study	1.00	1.66	1.40	1.13	1,138 borehole models in China
Mean values	1.00	1.41	1.30	1.20	
Median values	1.00	1.39	1.30	1.16	

Note: Data marked with # were excluded in statistics.

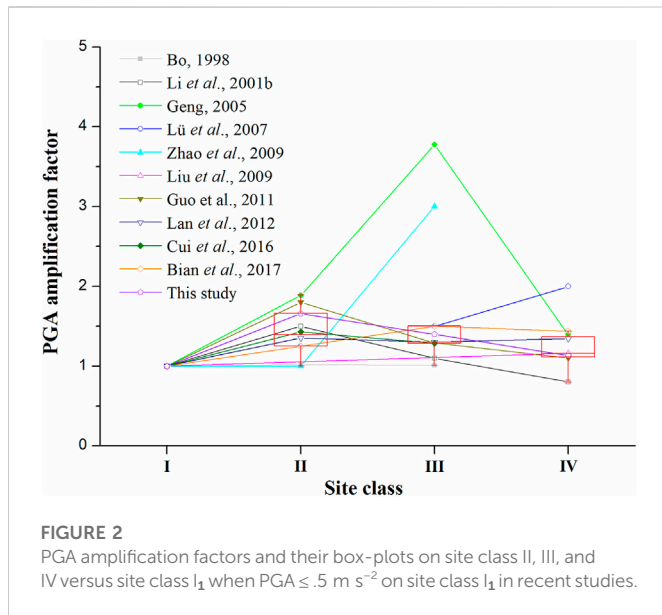


FIGURE 2
PGA amplification factors and their box-plots on site class II, III, and IV versus site class I when $PGA \leq 0.5 \text{ m s}^{-2}$ on site class I in recent studies.

4 Scaling ratios for PGA-normalized s_a

4.1 Data resource

The statistical data used in this section were from NGA-West two database of the next generation ground motion attenuation program of the Pacific Earthquake Engineering Research Center. NGA-West two database had collected and processed more than 20,000 strong motion records of shallow crustal earthquakes in

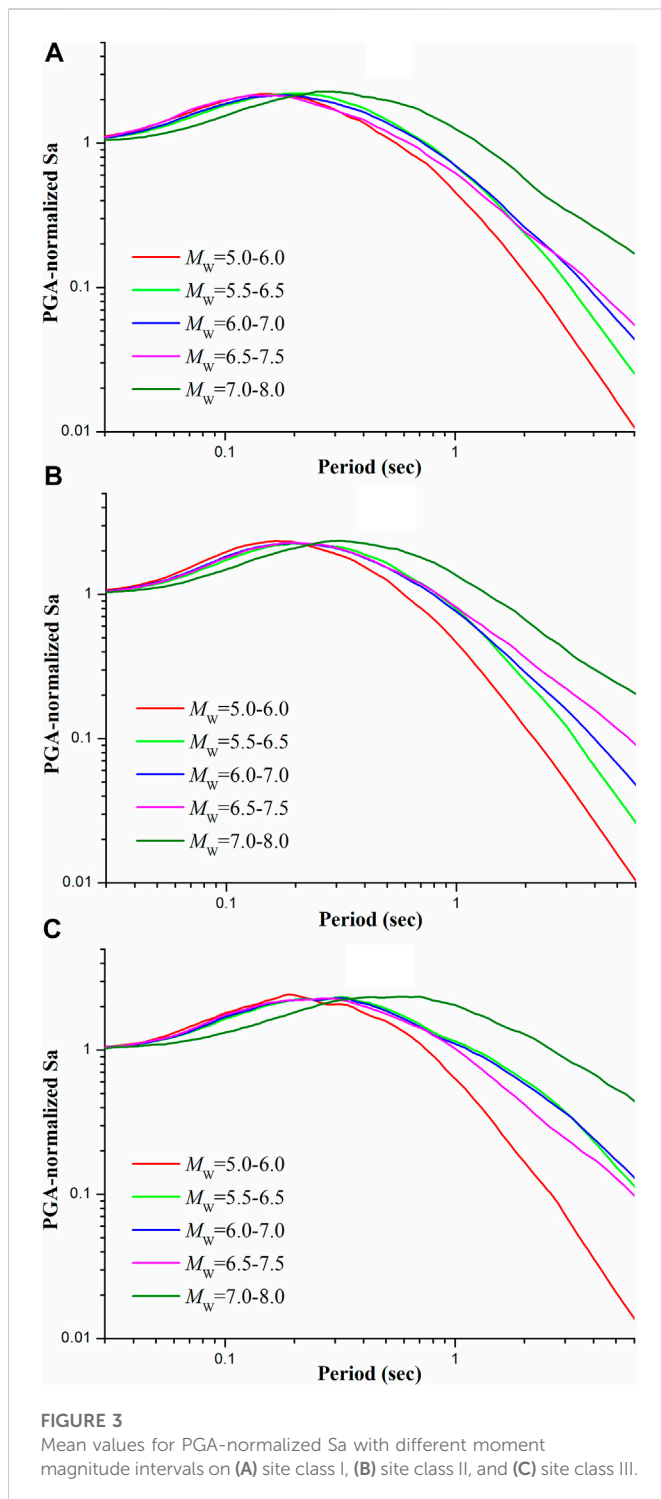
active tectonic regions around the world, including detailed earthquake parameters and site information. However, strong motion records in earthquakes above moment magnitude 8.0 were not included in this database. Although abundant strong motion records were obtained in the 2011 earthquake off the Pacific coast of Tōhoku, Japan, they were excluded in this study considering that this earthquake occurred in a marine subduction zone. Almost all the destructive earthquakes in China are of another type of earthquake mechanism, i.e., inland earthquakes. Researches had shown that there were significant differences between the ground motions of the two types of earthquake mechanism, and the long-period ground motions of earthquakes in marine subduction zone were significantly lower than the inland earthquakes.

Three thousand five hundred eighty four strong motion records with moment magnitude $M_w \geq 5.0$, Joyner-Boore distance (the closest distance to the surface projection of an extended seismogenic fault) $\leq 200 \text{ km}$, and $PGA \geq 0.3 \text{ m s}^{-2}$ were used. The sample capacities of records on each site class grouped by moment magnitude, Joyner-Boore distance or PGA were listed in Table 4. There were most strong motion records on site class II, and their distribution was relatively uniform grouped by moment magnitude, Joyner-Boore distance or PGA. There were fewer records on site class I and site class III, and only 30 records on site class IV.

According to the lowest usable frequency of each strong motion record given by NGA-West2 database, the S_a values exceeding the corresponding period were eliminated. Consequently, 100% of the 3,584 records were used in the statistics of S_a when period $T \leq 1.0 \text{ s}$, while 97.0% when $1.0 \text{ s} < T \leq 2.0 \text{ s}$, 80.9% when $2.0 \text{ s} < T \leq 4.0 \text{ s}$, and 70.1% when $4.0 \text{ s} < T \leq 6.0 \text{ s}$.

TABLE 4 Sample capacities of records from NGA-West2 database on each site class.

Consideration	Interval	Site class I	Site class II	Site class III	Site class IV
Moment magnitude	5.0–5.5	81	303	22	0
	5.5–6.0	114	294	35	0
	6.0–6.5	227	463	206	1
	6.5–7.0	276	575	136	27
	7.0–7.5	76	272	29	0
	7.5–8.0	119	227	99	2
Joyner-Boore distance (km)	0–10	127	474	34	2
	10–30	271	460	75	6
	30–60	281	682	147	5
	60–100	158	364	172	4
	100–200	56	334	99	13
PGA ($\text{m}\cdot\text{s}^{-2}$)	.3–0.5	209	576	157	10
	.5–1.0	286	610	193	9
	1.0–2.0	217	581	117	6
	2.0–4.0	133	252	44	4
	>4.0	48	115	16	1
Total		893	2,134	527	30



4.2 PGA-normalized Sa

The PGA-normalized Sa was defined as the quotient of Sa with 5% damping ratio divided by PGA of each strong motion record. The site condition represented by the site class, earthquake magnitude represented by the moment magnitude M_w , source distance represented by the Joyner-Boore distance, and ground motion strength represented by PGA, were selected as the key influences on PGA-normalized Sa in this study, for they significantly affected Sa.

Only PGA-normalized Sa on site class I, II, and III was analysed due to the small sample capacity of records on the site class IV.

The mean values of PGA-normalized Sa with different moment magnitude intervals were shown in Figure 3, which indicated that:

- 1) PGA-normalized Sa was significantly affected by the moment magnitude.
- 2) Generally, the medium-to-long period ($T > .20$ s on site class I, $T > .24$ s on site class II, and $T > .30$ s on site class III) segments of PGA-normalized Sa remarkably increased with the increase of the moment magnitude.
- 3) The short period ($T < .20$ s on site class I, $T < .24$ s on site class II, and $T < .30$ s on site class III) segments of PGA-normalized Sa with moment magnitude $M_w = 5.0-7.5$ were almost identical to each other, while their values were slightly larger than the values with moment magnitude $M_w = 7.0-8.0$.
- 4) The differences among the PGA-normalized Sa with moment magnitude $M_w = 5.5-6.5$, $6.0-7.0$, and $6.5-7.5$, were much slighter comparing the differences among other moment magnitude intervals. It might be caused by the geometry of seismogenic faults, which could be simplified to be a point source in a small earthquake, an area source of several square kilometers in a medium earthquake, and a rectangle source tens to more than 100 km long in a great earthquake.
- 5) The medium period ($.30 \text{ s} < T < 3.00 \text{ s}$) segments on site class I, and long period ($T > 1.00 \text{ s}$) segments on site class III with moment magnitude $M_w = 6.5-7.5$, were abnormally small.

The mean values of PGA-normalized Sa with different Joyner-Boore distance intervals and with different PGA intervals were shown in Figure 4. It could be concluded that:

- 1) PGA-normalized Sa was slightly affected by the Joyner-Boore distance or PGA comparing with the influence caused by the moment magnitude.
- 2) From a global perspective, the medium-to-long period segments of PGA-normalized Sa increased with the increase of Joyner-Boore distance, and decreased with the increase of PGA in an imperceptible degree.

4.3 Residual analyses after removing the influence of moment magnitude

In order to further analyse the dependence of the PGA-normalized Sa on the source distance and the ground motion strength, residual analyses were used to remove the influence of the most significant influence factor, namely moment magnitude. According to the moment magnitude and site class corresponding to each strong motion record, fitting values of PGA-normalized Sa of the record were obtained from the data shown in Figure 3 using linear interpolation under logarithmic coordinates. By subtracting the fitting values from the calculated PGA-normalized Sa of each strong motion record, the residuals of logarithmic PGA-normalized Sa were obtained.

The residuals of logarithmic PGA-normalized Sa with different Joyner-Boore distance intervals were shown in Figures 5A–C, which indicated that:

- 1) The regularity of residual curves with the Joyner-Boore distance on site class I, II and III was weak, which meant that PGA-normalized Sa and the Joyner-Boore distance had weak correlation.

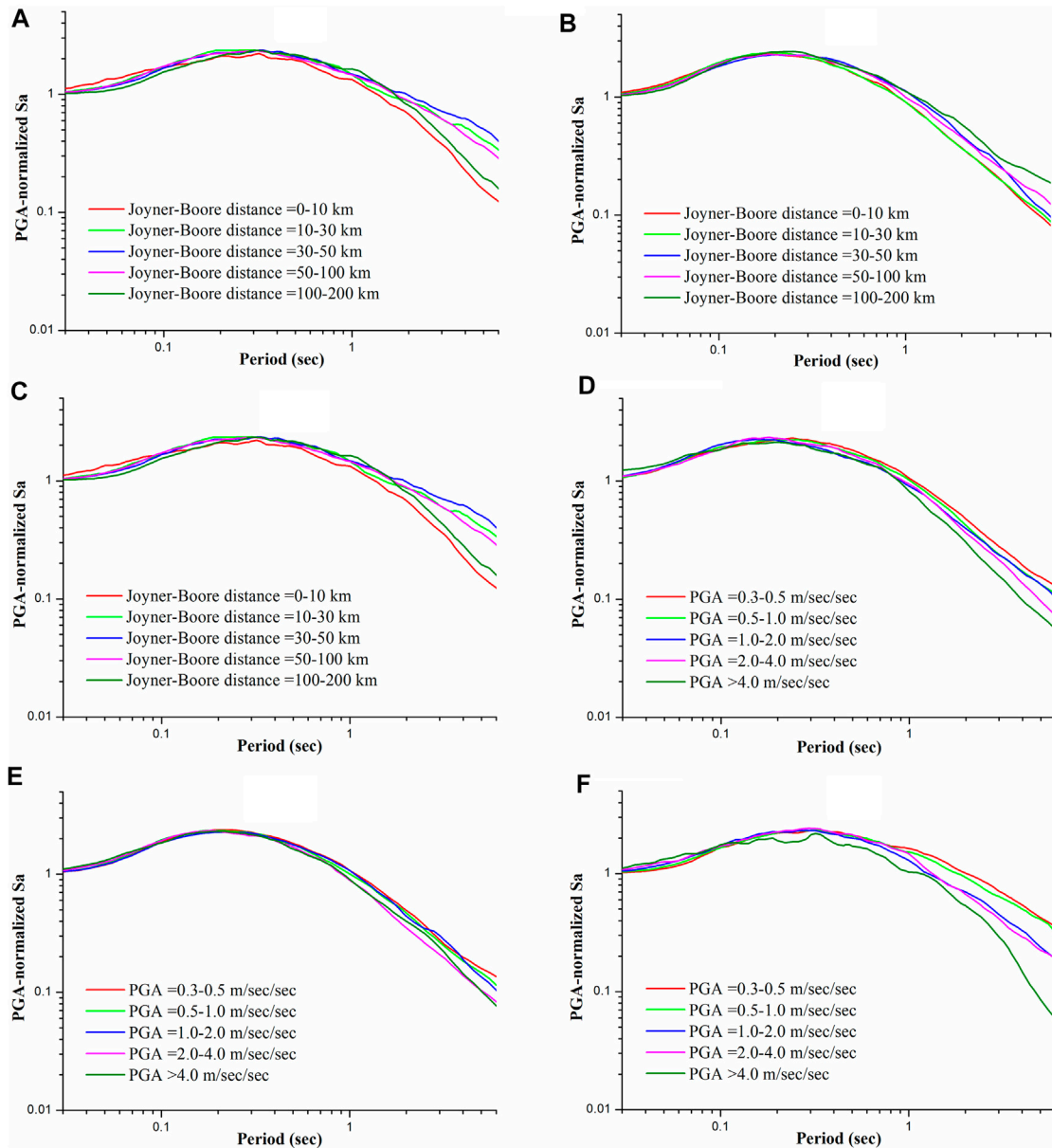


FIGURE 4

Mean values for PGA-normalized S_a with different Joyner-Boore distance intervals on (A) site class I, (B) site class II, (C) site class III, and mean values for PGA-normalized S_a with different PGA intervals on (D) site class I, (E) site class II, and (F) site class III.

- 2) The discreteness of residuals caused by the Joyner-Boore distance was sufficiently small, within $10^{\pm .1}$ on site class I and II, as well as on site class III when $T \leq 20$ s.

The residuals of logarithmic PGA-normalized S_a with different PGA intervals were shown in Figures 5D–F, which indicated that:

- 1) When $T < .20$ s, the discreteness of residuals caused by PGA was within $10^{\pm .05}$ on site class I, II, and III.
- 2) When $T > .30$ s, the residuals regularly decreased with the increase of PGA; meanwhile, the differences among the residuals with different PGA intervals gradually increased with the increase of periods.

Comparisons of the residuals in Figure 5 showed that the PGA-normalized S_a was much more significantly correlated with PGA than with the Joyner-Boore distance. In other words, PGA was a more sensitive variable than the Joyner-Boore distance in the determination of PGA-normalized S_a .

Incidentally, PGA and the Joyner-Boore distance were not completely independent variables in an earthquake, for PGA was negatively correlated with the source distance statistically as a result of the strong motion attenuation. Meanwhile, on rock sites with small source distances, the long-period S_a normalized by PGA was known to be smaller than that on the rock sites with large source distances; but at the same time, stronger non-linearity of overburden layers would amplify the long-period S_a on soil sites with smaller source distances. The influences on PGA-

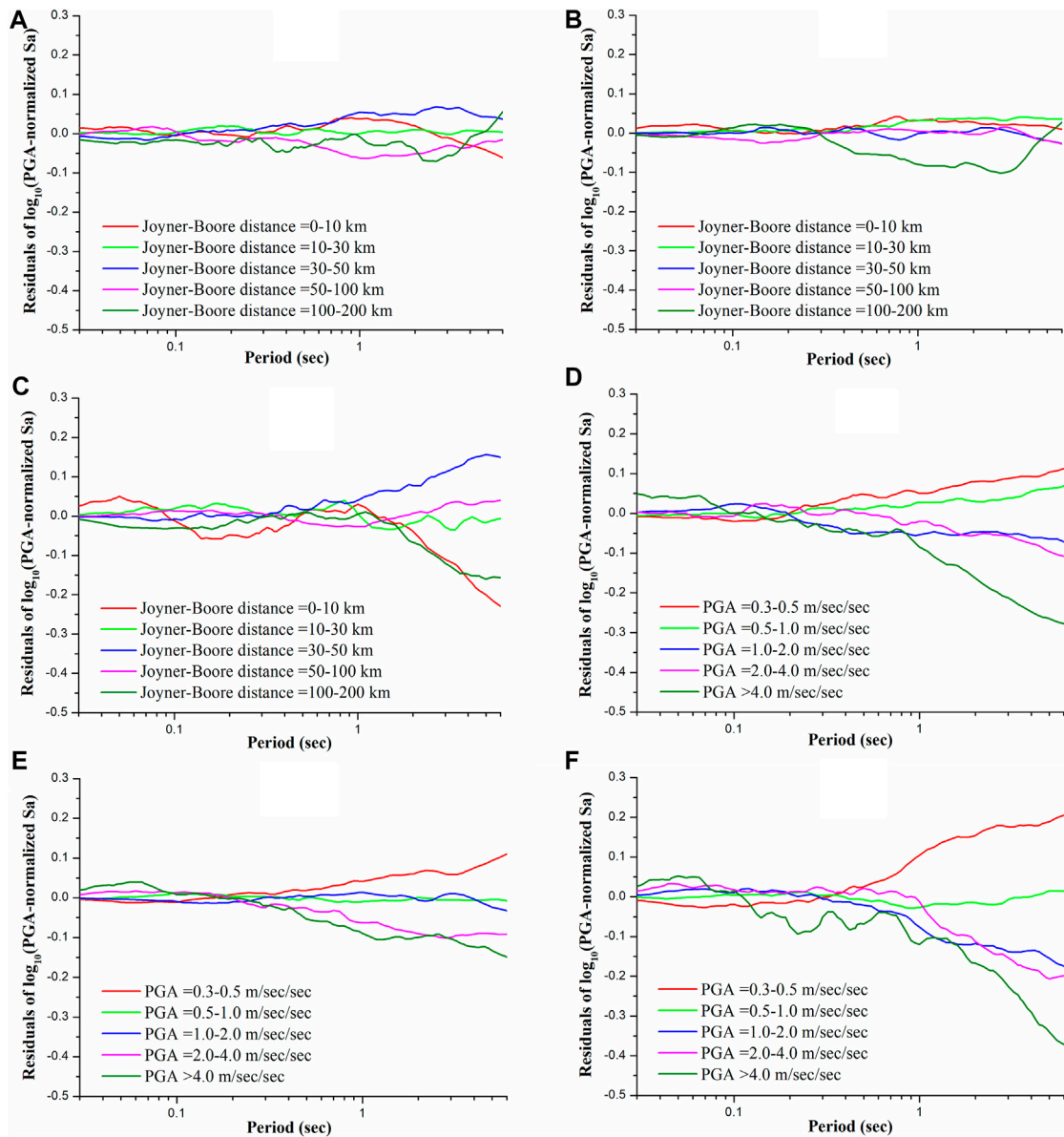


FIGURE 5 Residuals of logarithmic PGA-normalized Sa with different Joyner-Boore distance intervals on (A) site class I, (B) site class II, (C) site class III, and residuals of logarithmic PGA-normalized Sa with different PGA intervals on (D) site class I, (E) site class II, and (F) site class III.

normalized Sa caused by PGA and source distance, which offset each other, were a subject worthy of further study.

4.4 Scaling ratios for PGA-normalized Sa on site class II and III

The quotients of PGA-normalized Sa on site class II and III divided by PGA-normalized Sa on site class I with each moment magnitude interval were shown in Figures 6A, B, which indicated that:

- 1) When $T < 1.00$ s, the quotients with different moment magnitude intervals on the same site class were identical to each other within acceptable deviations.
- 2) When $T > 1.00$ s, the deviations of the quotients with different moment magnitude intervals increased with the increase of

periods, and this trend was more significant on site class III than on site class II.

The above phenomenon could be explained by Figure 5, which showed that the Joyner-Boore distance and PGA significantly affected the PGA-normalized Sa when $T > 1.00$ s. Further considerations of the Joyner-Boore distance and PGA during the calculation would probably lower the deviations.

In order to eliminate the impact of source spectra differences in different earthquakes, earthquakes with no less than five strong motion records on site class I as well as on site class II or III were selected. The quotients of PGA-normalized Sa on site class II or III divided by PGA-normalized Sa on site class I in the same selected earthquake, and their mean values weighted by square roots of the sample capacities on site class I and on site class II or III, were shown in Figures 6C, D, which indicated that:

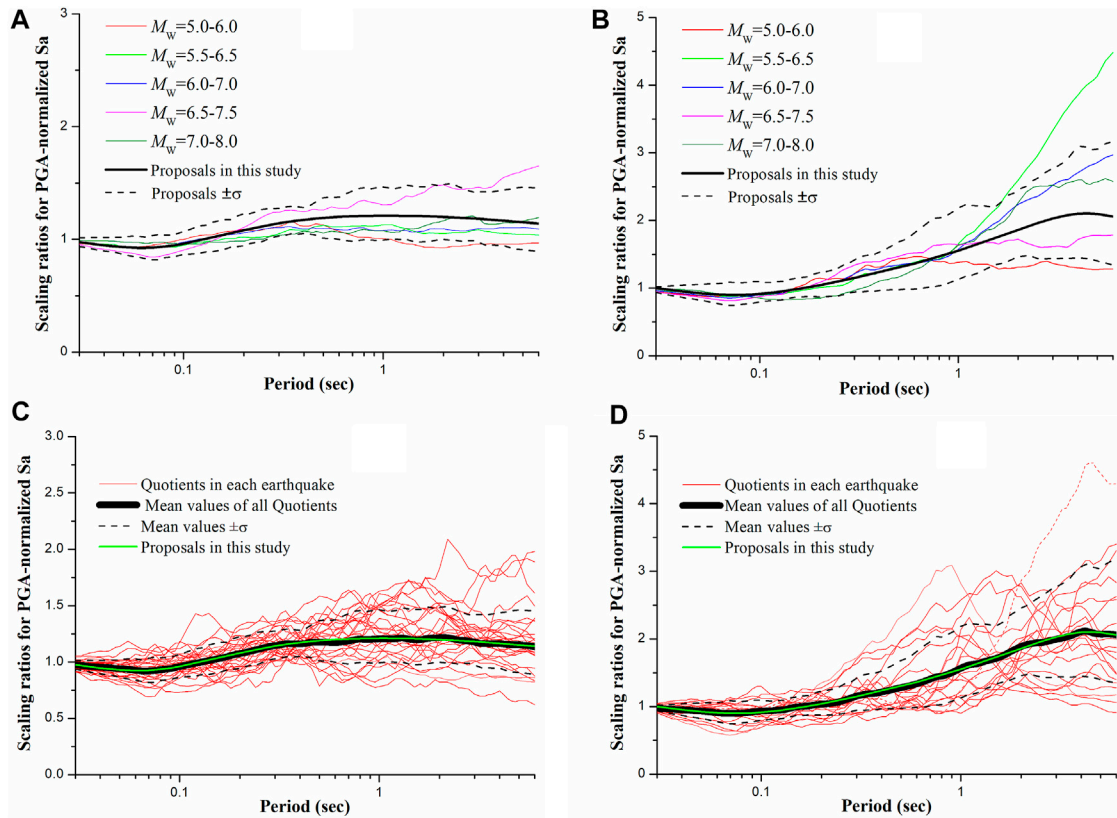


FIGURE 6 Quotients of PGA-normalized Sa on (A) site class II, (B) site class III divided by PGA-normalized Sa on site class I with different moment magnitude intervals, and quotients of PGA-normalized Sa on (C) site class II, (D) site class III divided by PGA-normalized Sa on site class I in the same selected earthquake. The scaling ratios proposed in this study were shown in green curves.

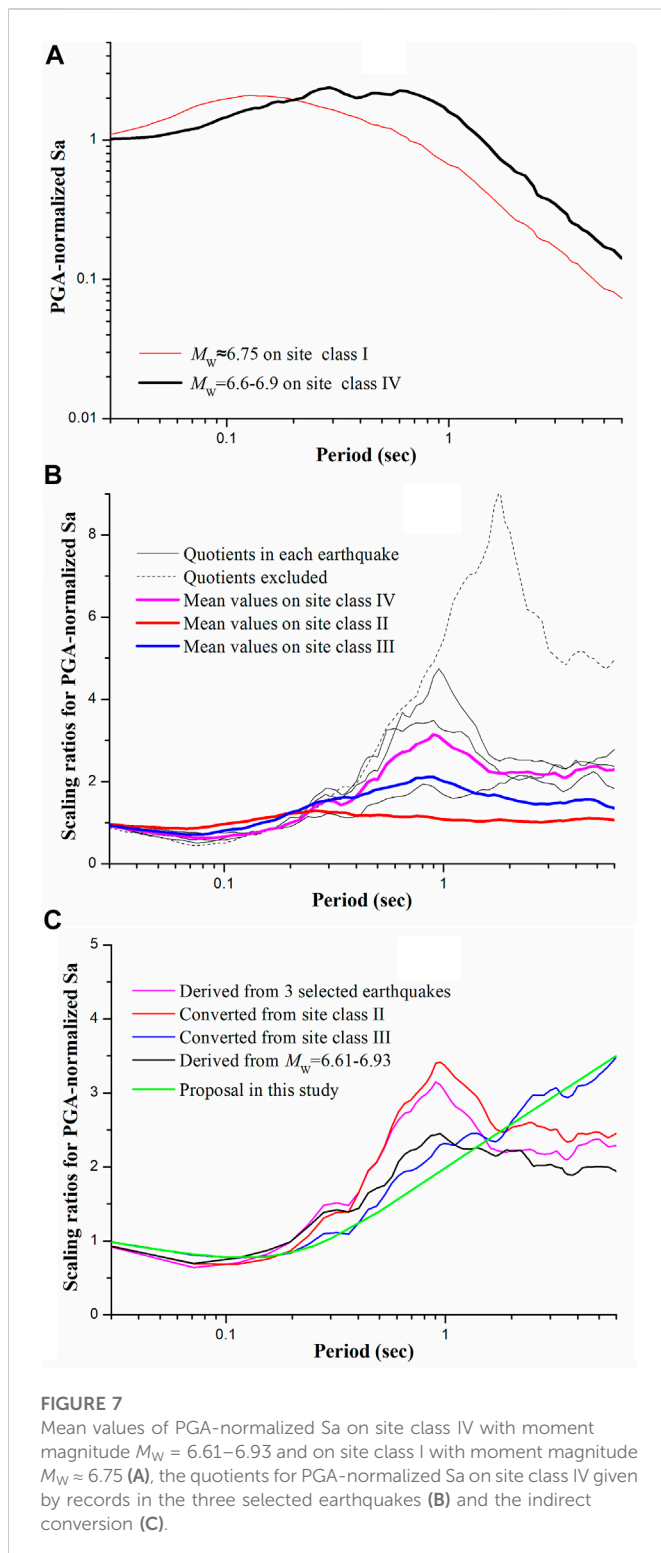
- 1) The deviations of the quotients calculated in the same selected earthquake were obviously larger than the deviations of quotients calculated in the same moment magnitude intervals shown in Figures 6A, B.
- 2) The mean values of quotients calculated in the same selected earthquake were almost identical to the average quotients calculated in the same moment magnitude intervals shown in Figures 6A,B.

The smoothen fittings for the mean values of quotients in Figures 6C,D were proposed as the scaling ratios of PGA-normalized Sa on site class II and III versus on site class I₁ in this study, which were shown as green curves. The proposed scaling ratios of PGA-normalized Sa could reflect the average impact of site conditions on spectral compositions on site class II and III as shown in Figures 6A,B, but in a particular earthquake, it would yield great error as shown in Figures 6C,D. As a consequence, the proposed scaling ratios could be used to estimate the seismic site effect for general projects with large quantities and wide areas with an acceptable accuracy in a statistical sense, but they would be non-negligible inaccurate on a particular engineering site in a particular earthquake.

4.5 Scaling ratios for PGA-normalized Sa on site class IV

The PGA-normalized Sa with different moment magnitude intervals on site class IV could not be reliably obtained because of the small sample capacity of only 30 strong motion records as listed in Table 4. So 26 strong motion records with moment magnitude $M_W = 6.61-6.93$ were used to calculate the PGA-normalized Sa on site class IV for second best as shown in Figure 7A. Meanwhile, the average PGA-normalized Sa on site class I with moment magnitude $M_W \approx 6.75$, which was the average moment magnitude of the 26 records on site class IV, were also calculated as shown in Figure 7A. The quotients of PGA-normalized Sa on site class IV with moment magnitude $M_W = 6.61-6.93$ divided by PGA-normalized Sa on site class I with moment magnitude $M_W \approx 6.75$ were shown as a black curve in Figure 7C as a black curve.

Four earthquakes with no less than five strong motion records on site class I as well as on site class IV were selected to eliminate the impact of source spectra differences, one of which was excluded in the calculation of mean values because of the excessive deviation. The quotients of PGA-normalized Sa on site class IV divided by PGA-normalized Sa on site class I in the same selected earthquake, and their mean values weighted by square roots of the sample



capacities on site class I and on site class IV were shown in Figure 7B, which indicated that:

- 1) The deviations of the quotients calculated in the same selected earthquake on site class IV were even much larger than these on site class III as shown in Figure 6D.

- 2) There was an obvious peak at $T = .90$ s on the curve of average quotients on site class IV. The period of this peak was inconsistent with the result on site class III as shown in Figure 6D.

In order to distinguish whether the obvious difference between the scaling ratios on site class IV and on site class III were caused by the source spectra of selected earthquakes, the mean values of quotients given by records in the three selected earthquakes on site class II and on site class III were also given in Figure 7B. It indicated that the trend of quotients on site class III given by records in the three earthquakes was comparable with quotients on site class IV, but significantly different from the scaling ratios on site class III given in Figure 6D. So it could be concluded that the uniqueness of source spectra in the three earthquakes might be the reason for this different trend.

Consequently, the quotients of PGA-normalized Sa on site class IV versus on site class I by an indirect conversion to eliminate the uniqueness of source spectra were shown in Figure 7C. To be more specific, the mean values of quotients of PGA-normalized Sa on site class IV in Figure 7B were divided by the quotients of PGA-normalized Sa on site class II or III in Figure 7B, and then multiplied the scaling ratios on site class II or III given in Figure 6C or Figure 6D. It could be concluded that:

- 1) The quotients calculated by 26 strong motion records with moment magnitude $M_w = 6.61-6.93$ were smaller than the mean values of quotients calculated by records in three selected earthquakes and the quotients converted from site class II. But the three of them shared the same trend, i.e., a peak at period $T = .90$ s, and relatively small values when period $T > 2.00$ s.
- 2) The quotients converted from site class III showed a very different trend, but they were comparable with the scaling ratios on site class III in Figure 6D.

Since the classification criteria for the site class IV were close to the site class III only with a smaller equivalent shear-wave velocity and a larger overburden thickness as listed in Table 1, and the peak at period $T = .90$ s was probably caused by unique source spectra, we proposed the smoothed quotients converted from site class III to be the scaling ratios for PGA-normalized Sa on the site class IV, which were shown in a green curve in Figure 7C.

5 Non-linear decay exponents

5.1 Data resource

More than 140,000 strong motion records at 137 stations in KiK-net (Kiban Kyoshin Network) were used in this section. The maximum peak acceleration of downhole records at each station $\geq 0.75 \text{ m s}^{-2}$. According to the site condition classification criteria in China listed in Table 1, 15 stations were on site class I₁, 107 stations were on site class II, 12 stations were on site class III, and only three stations were on site class IV.

5.2 Non-linear decay of surface/borehole Sa

The quotients of Sa on the ground surface divided by Sa in the borehole, i.e., surface/borehole (S/B) Sa, obtained in the same earthquake of each station were calculated, and then the average platform value of surface/borehole Sa were determined using the similar concept as the

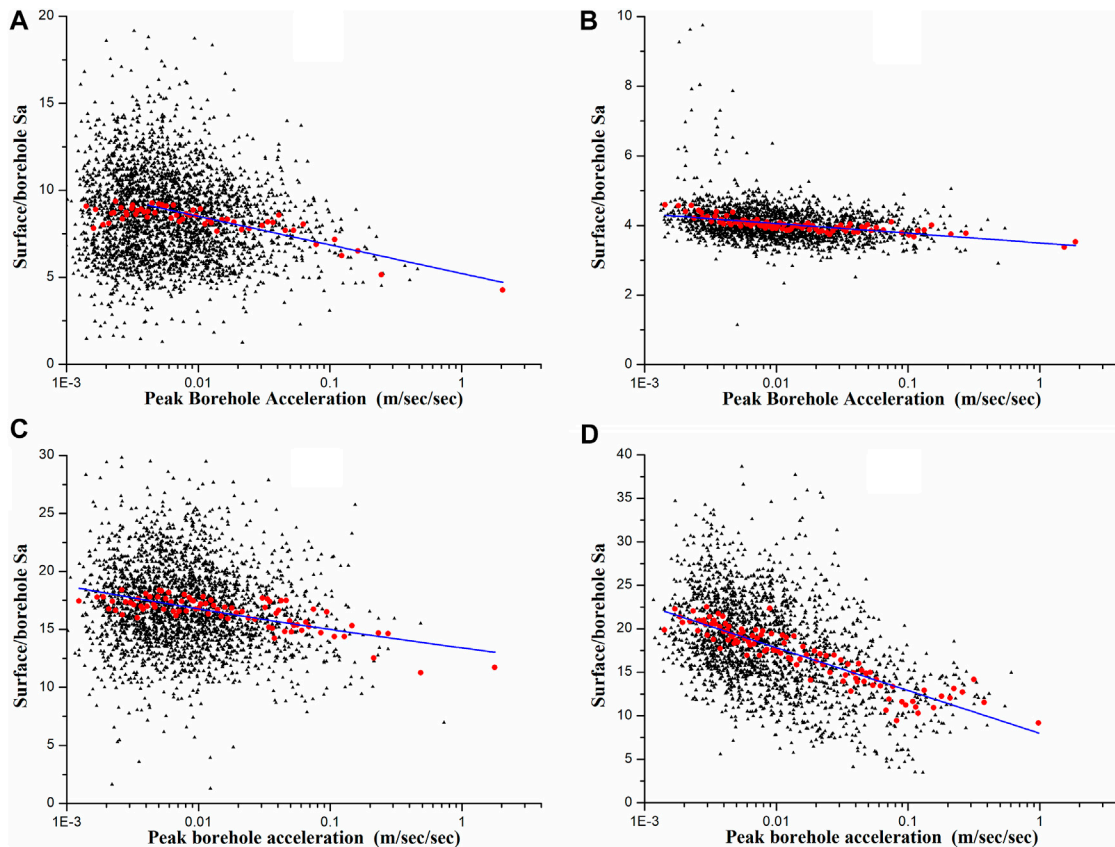


FIGURE 8

The scatter diagrams, their smoothed mean values, and linear fittings for the platform values of surface/borehole S_a at (A) Station TCGH10 on site class I_1 , (B) Station FKSH11 on site class II, (C) Station TCGH16 on site class III, and (D) Station IBRH10 on site class IV.

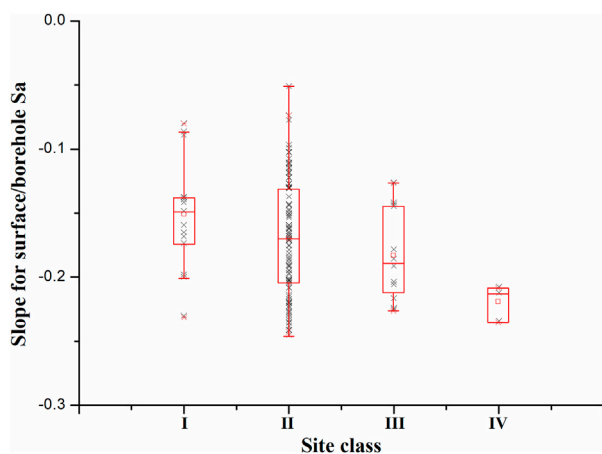


FIGURE 9

The scatter diagrams and box-plots for the slopes of the linear fittings for platform values of surface/borehole S_a for all the 137 stations on each site class.

calculation of EPA but at a variable period range (Ding et al., 2021). The scatter diagrams of the average platform values at four stations were shown in Figure 8, which indicated that large discreteness still could not

hide the decay trend with strong motion strength. The mean values of the platform values in a variable sample capacity window narrowing with the increase of the strong motion strength were also shown in Figure 8 as red bold dots, which showed a clearer linear decay trend under semi-logarithmic coordinates than the platform values shown in black dots.

The slopes of the linear fittings for platform values at all the 137 station were shown in Figure 9, which indicated that the slopes were smaller on sites with softer and thicker overburdens, even though there was considerable overlap between two adjacent site classes.

5.3 Proposed non-linear decay exponents

The median slopes of the linear fittings for platform values of surface/borehole S_a under semi-logarithmic coordinates, i.e., -0.150 on site class I_1 , -0.169 on site class II, -0.182 on site class III, and -0.218 on site class IV, were proposed as the non-linear decay exponents of S_a as a temporary compromise. The non-linear decay exponents on site class I_0 was proposed to be 0.

The non-linear decay exponents should be derived from the quotients of S_a on soil sites divided by S_a on rock sites, namely, soil/rock S_a , under the same strong motion inputs, or at least when the distance between the soil site and the rock site was negligible compared with their source distance. There would be an error induced by the assumption that the non-linear decay exponents of surface/borehole

TABLE 5 Scaling ratios for Sa due to site conditions varying with PGA on site class I₁.

Sa	Site class	PGA on site class I ₁ (m s ⁻²)					
		≤0.5	1.0	1.5	2.0	3.0	≥4.0
PGA (T = 0 s)	I ₀	.80	.84	.86	.87	.89	.91
	I ₁	1.00	1.00	1.00	1.00	1.00	1.00
	II	1.39	1.38	1.38	1.37	1.37	1.37
	III	1.30	1.29	1.28	1.27	1.27	1.26
	IV	1.16	1.14	1.12	1.11	1.10	1.09
T = .3 s	I ₀	.80	.84	.86	.87	.89	.91
	I ₁	1.00	1.00	1.00	1.00	1.00	1.00
	II	1.59	1.58	1.57	1.57	1.56	1.56
	III	1.49	1.48	1.47	1.47	1.46	1.45
	IV	1.19	1.17	1.16	1.15	1.13	1.12
T = 1.0 s	I ₀	.80	.84	.86	.87	.89	.91
	I ₁	1.00	1.00	1.00	1.00	1.00	1.00
	II	1.68	1.67	1.67	1.66	1.66	1.65
	III	2.01	2.00	1.98	1.98	1.96	1.96
	IV	2.31	2.26	2.23	2.21	2.19	2.17
T = 3.0 s	I ₀	.80	.84	.86	.87	.89	.91
	I ₁	1.00	1.00	1.00	1.00	1.00	1.00
	II	1.64	1.63	1.63	1.62	1.62	1.61
	III	2.64	2.61	2.60	2.59	2.57	2.56
	IV	3.39	3.32	3.28	3.25	3.21	3.18

Sa were identical to soil/rock Sa. But as there were not sufficient number of samples to obtain soil/rock Sa, the slopes of the linear fittings for platform values of surface/borehole Sa might be approximately regarded to be the non-linear decay exponents of soil/rock Sa (Li et al., 2021).

6 Proposed scaling ratios for sa

According to the scaling ratios for PGA, scaling ratios for PGA-normalized Sa, and non-linear decay exponents given by above statistics, the scaling ratios for Sa on site class I₀, I₁, II, III, and IV were proposed as following:

$$F_i(T, PGA_{I_1}) = \alpha_i \beta_i(T) \left[1 + (\gamma_i - \gamma_{I_1}) \log_{10} \frac{PGA_{I_1}}{0.5} \right] \quad (4)$$

where the site class $i = I_0, I_1, II, III, \text{ or } IV$; T was the period in second; PGA_{I_1} was the peak ground acceleration on site class I₁ in m s⁻²; $F_i(T, PGA_{I_1})$ were the scaling ratios for Sa at period T on site class i when the peak ground acceleration on site class I₁ was PGA_{I_1} ; scaling

ratio for PGA $\alpha_i = .80, 1.00, 1.39, 1.30, \text{ or } 1.16$ for $i = I_0, I_1, II, III, \text{ or } IV$ when $PGA_{I_1} = .5 \text{ m s}^{-2}$; non-linear decay exponent $\gamma_i = .000, -.150, -.169, -.182, \text{ or } -.218$ for $i = I_0, I_1, II, III, \text{ or } IV$; scaling ratios for PGA-normalized Sa, $\beta_i(T)$, were shown in Figures 6C, D, 7C in green curves for $i = II, III, \text{ or } IV$, and $\beta_i(T) \equiv 1$ for $i = I_0$ and I_1 .

The scaling ratios for PGA, Sa ($T = .30 \text{ s}$), Sa ($T = 1.00 \text{ s}$), and Sa ($T = 3.00 \text{ s}$) varying with PGA_{I_1} were listed in Table 5, and the curves of scaling ratios for Sa when $PGA_{I_1} = .5, 1.0, 1.5, 2.0, 3.0, 4.0 \text{ m s}^{-2}$ and their corresponding values in “GB18306: Seismic ground motion parameters zonation map of China” (Ministry of Housing and Urban-Rural Development of the People’s Republic of China, General Administration of Quality Supervision, Inspection and Quarantine of the People’s Republic of China, 2010) were shown in Figure 10, which indicated that:

- 1) The non-linearities of scaling ratios for Sa varying with strong motion strength on site class I₁ were imperceptibly indeed comparing with GB18306. One reason for this phenomenon was the consideration of non-linearity on site class I₁ in this study, and another possible reason was that the non-linear decay exponents for soil/rock Sa were not identical to the non-linear decay exponents for surface/borehole Sa.
- 2) The scaling ratios for Sa on site class II, the scaling ratios for Sa at $T < .4 \text{ s}$ on site class III when $PGA_{I_1} \leq 2.0 \text{ m s}^{-2}$, and the scaling ratios for Sa at $T < .6 \text{ s}$ on site class IV when $PGA_{I_1} \geq 3.0 \text{ m s}^{-2}$, were comparable with GB18306.
- 3) The scaling ratios for Sa at $.4 \text{ s} < T < 2.0 \text{ s}$ on site class III, and the scaling ratios for Sa at $.6 \text{ s} < T < 2.0 \text{ s}$ on site class IV were smaller than or comparable with GB18306, while the scaling ratios for Sa at $T > 2.0 \text{ s}$ on site class III and IV were obviously larger than GB18306.

To sum up, the non-linearity of scaling ratios for Sa on site class I₁ was non-ignorable, and the proposed scaling ratios on site class II were comparable with GB18306, meanwhile the proposed scaling ratios on site class III and IV were smaller at medium periods $.5 \text{ s} < T < 2.0 \text{ s}$ and larger at long periods $T > 2.0 \text{ s}$ than GB18306.

7 Conclusion and discussions

Based on numerical simulations of 1,138 borehole models in China, 3,584 strong motion records in NGA West two database, and about 140 thousand borehole observation data recorded by KiK-net, a novel approach assembled by scaling ratios for PGA, scaling ratios for PGA-normalized Sa, and non-linear decay exponents, was proposed.

- 1) The scaling ratios for PGA derived from numerical simulations of borehole models when motions were not so strong were acceptable, but one-dimensional equivalent linearization method might overestimate the non-linearity of soil when motions were strong enough for engineering significance.
- 2) The scaling ratios for PGA-normalized Sa derived from the strong motion records in NGA-West two database could reflect the average impact of site conditions on spectral compositions, but they would yield great errors in a particular earthquake on an actual site.
- 3) The non-linear decay exponents of surface/borehole Sa were negatively correlated with site classes, and the non-linear decay exponent on site class I₁ was non-ignorable.

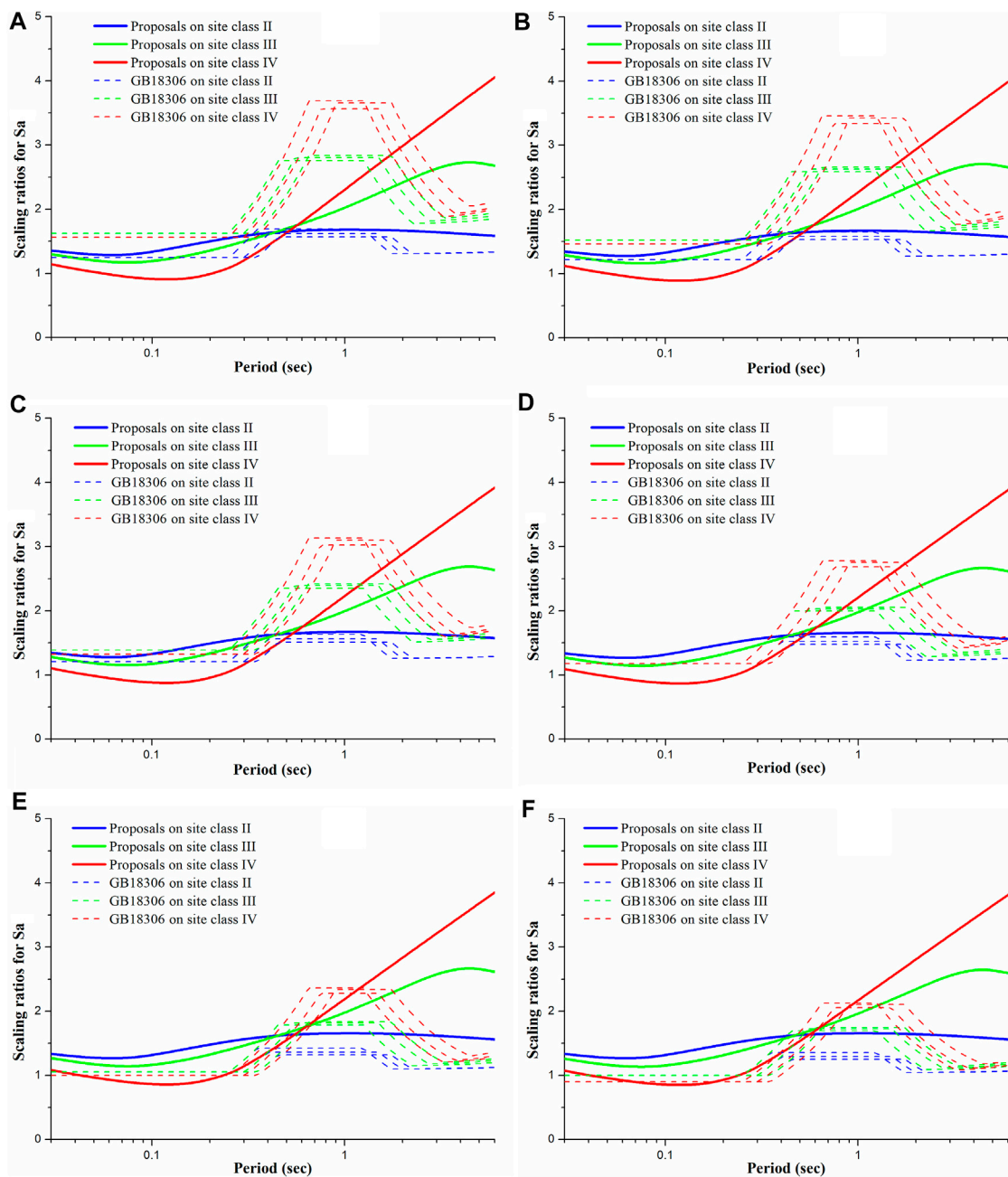


FIGURE 10

Scaling ratios for Sa on site class II, III, and IV when PGA on site class I₁ (A) $\leq 5 \text{ m s}^{-2}$, (B) $= 1.0 \text{ m s}^{-2}$, (C) $= 1.5 \text{ m s}^{-2}$ (D) $= 2.0 \text{ m s}^{-2}$, (E) $= 3.0 \text{ m s}^{-2}$, and (F) $\geq 4.0 \text{ m s}^{-2}$.

4) The scaling ratios for Sa proposed in this study offered an option to determine the impact on Sa caused by seismic site effect on each site class under site condition classifications in China.

Further improvements were also needed to improve the reliability and applicability of the proposed scaling ratios for Sa.

1) The influences of the source distance and the strong motion strength on PGA-normalized Sa needed more considerations.

2) The strong motions on site class I₀ and on site class I₁ should be distinguished in detail, especially in the determination of non-linear decay exponents. Ignorance of non-linearity on site class I₁ might significantly affect the non-linearity of scaling ratios for Sa on all the site classes, which was a common problem in recent studies and current regulations.

3) The non-linear decay exponents of soil/rock Sa needed to be built considering the inconsistency between the soil/rock Sa and surface/borehole Sa.

4) Additionally, scaling ratios on site class IV needed to be paid more attentions because of limited sample capacity.

Data availability statement

The original contributions presented in the study are included in the article/[Supplementary Material](#), further inquiries can be directed to the corresponding author.

Author contributions

All authors listed have made a contribution to conception and design of the study, and approved it for publication. Scaling ratios for PGA: XL. Non-linear decay exponents: YD. Scaling ratios for PGA-normalized S_a and other sections: YW. Writing-original Draft: YW. Writing-reviewing and editing: YW and XL. All authors contributed to manuscript revision, read, and approved the submitted version.

Funding

This study is supported by the National Key R&D Program of China (2022YFC3003503) and National Natural Science Foundation of China (52192675).

Acknowledgments

We acknowledge with thanks the strong motion data from KiK-net of National Research Institute for Earth Science and

References

- Aki, K. (1993). Local site effects on weak and strong ground motion. *Tectonophysics* 218 (1-3), 93–111. doi:10.1016/0040-1951(93)90262-i
- Bian, F. D., and Ding, H. P. (2017). Estimation and application of depth correction factor for site coefficient based on KiK-net strong-motion seismograph network. *J. Suzhou Univ. Sci. Technol. Eng. Technol.* 30 (4), 1456–1519.
- Bo, J. S., Li, Q., Qi, W. H., Yuting, W., Xinlong, Z., et al. (2021). Research progress and discussion of site condition effect on ground motion and earthquake damage. *J. Jilin Univ. (Earth Sci. Ed.)* 51 (5), 1295–1305.
- Bo, J. S. (1998). *Site classification and design response spectrum adjustment method*. Harbin, China, Earthquake Administration: Institute of Engineering Mechanics.
- Boore, D. M. (2004). Estimating $s(30)$ (or NEHRP site classes) from shallow velocity models (depths < 30 m). *Bull. Seismol. Soc. Am.* 94 (2), 591–597. doi:10.1785/0120030105
- Cui, H., and Ding, H. P. (2016). Estimation of site coefficient based on KiK-net strong-motion seismograph network. *Earthq. Eng. Eng. Vib.* 36 (4), 147–152.
- Ding, Y., Wang, Y. S., Wang, N., et al. (2021). Study on nonlinear statistical characteristics of surface/downhole response spectrum ratio and influencing factors. *Technol. Earthq. Disaster Prev.* 16 (2), 362–370.
- General Administration of Quality Supervision, Inspection and Quarantine of the People's Republic of China (2016). *Seismic ground motion parameters zonation map of China* (Beijing, China: China Quality and Standards Publishing & Media Co., Ltd), GB18306.
- Geng, S. W. (2005). *Strong ground motion input parameter for seismic design*. Harbin, China, Earthquake Administration: Institute of Engineering Mechanics, 44–69.
- Guo, F., Wu, D. M., Xu, G. F., et al. (2011). Effect of site condition on the maximum value of seismic design response spectrum. *J. Civ. Eng. Manag.* 28 (1), 69–72.
- Hu, Y. X. (2006). *Earthquake engineering*. 2nd. Beijing, China: Seismological Press.
- Hu, Y. X., Sun, P. S., Zhang, Z. Y., et al. (1980). Effects of site conditions on earthquake damage and ground motion. *Earthq. Eng. Eng. Vib.* 0 (0), 34–41.
- Lan, J. Y., Lv, Y. J., and Liu, H. S. (2012). Influence of intensity and frequency of ground motion on site earthquake response. *Technol. Earthq. Disaster Prev.* 7 (1), 37–45.
- Disaster Resilience (NIED), and from NGA-West2 database of the Pacific Earthquake Engineering Research Center (PEER). We also owed sincere thanks to two reviewers for their constructive comments optimizing our statistical results.
- Li, X. J. (2013). Adjustment of seismic ground motion parameters considering site effects in seismic zonation map. *Chin. J. Geotechnical Eng.* 35 (S2), 21–29.
- Li, X. J., Li, N., Wang, J. K., et al. (2021). Difference between horizontal-to-vertical spectral ratio and surface-to-bedrock spectral ratio of strong-motion and modified horizontal-to-vertical spectral ratio method. *Technol. Earthq. Disaster Prev.* 16 (1), 81–90.
- Li, X. J., Pen, Q., and Liu, W. Z. (2001). Consideration of site effects for determination of design earthquake ground motion parameters. *Word Inf. Earthq. Eng.* 17 (4), 34–41.
- Li, X. J., and Peng, Q. (2001). Calculation and analysis of earthquake ground motion parameters for different site categories. *Earthq. Eng. Eng. Vib.* 21 (1), 29–36.
- Liu, Z., Shen, J. W., Shi, S. Z., et al. (2009). Soft soil amplification of peak ground acceleration. *J. Tongji Univ. Nat. Sci.* 37 (5), 607–611.
- Lü, H. S., and Zhao, F. X. (2007). Site coefficients suitable to China site category. *Acta Seismol. Sin.* 29 (1), 71–79. doi:10.1007/s11589-007-0071-6
- Lu, Y. J., Peng, Y. J., Lan, J. Y., et al. (2008). Some key problems about site effects on seismic ground motion parameters. *Technol. Earthq. Disaster Prev.* 3 (2), 126–135.
- Ministry of Housing and Urban-Rural Development of the People's Republic of China, General Administration of Quality Supervision, Inspection and Quarantine of the People's Republic of China, (2010). *Code for seismic design of buildings*. Beijing, China: China Architecture & Building Press, GB50011, 18–35.
- Seed, H. B., and Idriss, I. M. (1969). Influence of soil conditions on ground motions during earthquakes. *J. Soil Mech. Found. Div.* 95 (1), 99–137. doi:10.1061/jsfeaq.0001260
- Stewart, J. P., and Seyhan, E. (2013). *Semi-empirical nonlinear site amplification and its application in NEHRP site factors*. Oakland, CA, USA: University of California.
- Wang, Y., Li, X., Li, M., et al. (2022). Study on scaling ratios for spectral accelerations of ground motion due to site conditions. *Technol. Earthq. Disaster Prev.* 17 (3), 464–472.
- Zhao, Y., Guo, M. Z., Li, H. M., et al. (2009). Contrast analysis of effect of site condition on the maximum of design response spectra. *Seismol. Geol.* 31 (1), 186–196.

Conflict of interest

The authors declare that the research was conducted in the absence of any commercial or financial relationships that could be construed as a potential conflict of interest.

Publisher's note

All claims expressed in this article are solely those of the authors and do not necessarily represent those of their affiliated organizations, or those of the publisher, the editors and the reviewers. Any product that may be evaluated in this article, or claim that may be made by its manufacturer, is not guaranteed or endorsed by the publisher.

Supplementary material

The Supplementary Material for this article can be found online at: <https://www.frontiersin.org/articles/10.3389/feart.2022.1112202/full#supplementary-material>